Analysis of Size-Dependent Quantum Efficiency in AlGaInP Micro–Light-Emitting Diodes With Consideration for Current Leakage

Yi-Yang Li, Fang-Zhong Lin, Kuo-Lin Chi, Shao-Yi Weng, Guan-Ying Lee, Hao-Chung Kuo, *Fellow, IEEE*, and Chien-Chung Lin, *Senior Member, IEEE*

***Abstract*—This study fabricated and analyzed AlGaInP-based red micro–light-emitting diodes (LEDs) ranging from 2 to 15 μm in size. To collect photons from a single micro-LED at this scale, a solar cell chip near the micro-LEDs was used. Quantum efficiency decreased at a faster rate than that predicted by the standard ABC model under high currents, and a leakage current component was added to fully describe this phenomenon. The modified model can be used to extract valuable information regarding the micro-LEDs, such as the Shockley–Read–Hall coefficient. A size dependency analysis revealed that the bulk Shockley–Read–Hall coefficient and surface recombination velocity of the micro-LEDs were 6.81×10^7 1/sec and 5.99×10^4 cm/sec, respectively. Further analysis of the size-dependent recombination effect can help us solve the side wall problem and maximize the light output of AlGaInP-based micro-LEDs for ultrahigh-resolution displays.**

***Index Terms*—Display, leakage current, light-emitting diode, radiative recombination, quantum well device.**

I. Introduction

THE development of semiconductor-based micro–light-emitting diodes (micro-LEDs) has received considerable attention in the advanced display industry. Micro-LED-based monitors can surpass current technology in terms of scalability, efficiency, color purity, and self-emission. Micro-LED-based monitors require perfect performance of numerous tasks. Thus, several aspects, such as microassembly, mass transfer, epitaxial growth, and electronic circuitry, must be substantially improved [1], [2]. A full-color micro-LED display requires red, green, and blue subpixels on the same backplane and various active materials to generate these colors: InGaN for blue and green and AlGaInP or high–In content InGaN for red [3]–[8]. When the resolution of the display is increased for augmented and virtual reality, the size of the red, green, and blue subpixels must be lowered. For example, a monochromatic screen with a 2000-pixel-per-inch resolution would require a 12-μm pixel array. For the same resolution in a full-color screen, a sub-10-μm device would be required [6], [9]. For InGaN- and GaN-based blue and green materials, devices of 1 μm or smaller have been used [10], [11]. Reducing the size of AlGaInP-based materials is difficult because of its high surface recombination and carrier leakage [12]–[15]. Carrier leakage could be caused by the low carrier confining potential in AlGaInP-based heterojunctions; this leads to an increase in electrical current during the use of photonic devices [12]–[15]. To address the high surface recombination, numerous studies have attempted to improve devices through passivation, such as that achieved through atomic layer deposition, plasma-enhanced chemical vapor deposition (PECVD), and patterned polyimide or chemical treatments (e.g., sulfur treatment) [6], [8], [9] and [16]. PECVD SiO_2 has been an important passivation material in semiconductor industry. Due to the high surface recombination velocity in the GaAs based material and device's small dimension, it was known that the AlGaInP red micro LED needs to be passivated to prevent from current leakage. Some previous literatures have shown improved performances because of the SiO_2 passivation on the sidewall of GaAs related mesa-type devices (including AlGaInP red LEDs) [8], [17]–[20]. The effect of SiO_2 passivation comes from the prevention of oxidation in the cation atoms in III-V materials at the sidewall/air interface [20]. The small scale of the devices in this study makes it difficult to see any illumination result if no PECVD SiO_2 layer is used. Meanwhile, the PECVD SiO_2 can provide limited protection if a long-term operation is considered and an atomic layer deposition (ALD) SiO_2 could provide an even better lifetime [6]. In addition to fabrication methods, analytical models are used to obtain crucial information used for device optimization. Especially for AlGaInP-based and GaAs-based optoelectronic devices, radiative and nonradiative processes have been investigated through the use of various measurements (e.g., minority

Manuscript received November 15, 2021; revised December 20, 2021; accepted December 24, 2021. Date of publication December 28, 2021; date of current version January 7, 2022. This work was supported in part by the Ministry of Science and Technology of Taiwan under Grants MOST 110-2218-E-A49-012-MBK, MOST 107-2221-E-002-197-MY3, and MOST 110-2221-E-002-186-MY3. (*Corresponding author: Chien-Chung Lin*).

Yi-Yang Li, Fang-Zhong Lin, Kuo-Lin Chi, Shao-Yi Weng, and Guan-Ying Lee are with the Institute of Photonic System, College of Photonics, National Yang Ming Chiao Tung University, Tainan City 71150, Taiwan (e-mail: wilson0658@gmail.com; carson553507@gmail.com; azsx14523@gmail.com; weng66666666@gmail.com; stp93050@gmail.com).

Chien-Chung Lin was with the Institute of Photonic System, College of Photonics, National Yang Ming Chiao Tung University, Taipei 106, Taiwan. He is now with Graduate Institute of Photonics and Optoelectronics, National Taiwan University, Taipei 106, Taiwan (e-mail: chienchunglin@ntu.edu.tw).

Hao-Chung Kuo is with the Department of Photonics, National Yang Ming Chiao Tung University, Hsinchu 300, Taiwan (e-mail: hckuo@faculty.nctu.edu.tw).

This article has supplementary downloadable material available at https://doi.org/10.1109/JPHOT.2021.3138946, provided by the authors.

Digital Object Identifier 10.1109/JPHOT.2021.3138946

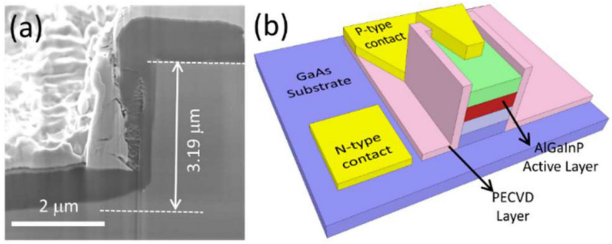

Fig. 1. (a) Scanning electron microscopy cross-section view of an AlGaInP micro-LED with a straight sidewall profile. (b) Schematic of a finished AlGaInP micro-LED.

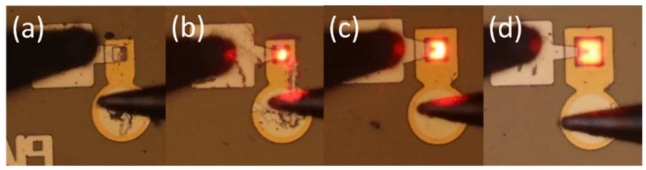

Fig. 2. Micro-LEDs at 100 A/cm^2 of current injection: (a) 2 μm, (b) 5 μm, (c) 10 μm, and (d) 15 μm.

carrier lifetime and high-pressure operations) and theories (e.g., efficiency and circuitry modeling) [12]–[14], [21]–[23]. The most popular model is based on the rate equations of an LED and is often called "the ABC model," which includes both radiative and nonradiative processes [22], [24]. We fabricated a series of small AlGaInP LEDs ranging from 2 to 15 μm in size and used a PECVD SiO_2 layer for sidewall passivation. The photonic characteristics of the devices, such as the quantum efficiency, indicated potential current leakage. A modified ABC model was created to determine the decrease in efficiency when we scaled down the AlGaInP devices.

II. Device Structure and Fabrication

The wafer was purchased from a vendor providing commercial AlGaInP wafers for red LEDs (Epileds Technologies, Tainan, Taiwan). A metal organic chemical vapor deposition system was used to deposit III–V-based semiconductor layers. As in our previous study [6], the p-type layer consisted of 2-μm GaP, and the active layer consisted of AlGaInP multiple quantum wells. The n-type layers consisted of 4-μm AlInP and AlGaInP layers. All epitaxial layers were grown on an n-type GaAs substrate. The standard semiconductor fabrication processes were applied [6], namely photolithography, inductively coupled plasma (ICP) etching, metal evaporation and liftoff, and deposition of the dielectric passivation layer. The device was square shaped, and the lengths of the sides were 2, 5, 10, and 15 μm. The gases used in the ICP dry etching were Cl_2, BCl_3, and Ar, and the etch rate was approximately 1 μm/min. The etch depth was between 3 and 4 μm, which is sufficient to penetrate the active layer and to isolate an individual device. By using ICP, we created a nearly straight side wall (approximately 88° according to scanning electron microscopy results) with little undercut in the top layer (Fig. 1(a)). The p-type metal was a Ti–Au composite (30 and 300 nm, respectively), and the n-type metal was a Cr–Au layer (30 and 300 nm, respectively). A 300-nm PECVD SiO_2 layer was used for sidewall protection and isolation. Fig. 1(b) presents the finished devices. The top surface of the mesa was partially covered by the p-type metal to conduct the electrical current and to not block the red photons completely. A rapid thermal annealing (RTA) step was added to the end of the process to enhance the device's IV characteristics. RTA was conducted at 350°C for 30 sec in a N_2 atmosphere. The devices were electrically characterized using a Keithley 2400 source meter, and their photonic properties were measured using a custom-made photodetection probe and an integrating sphere for optical spectrum acquisition. The optical output power of a micro LED on wafer was measured through the detection of photocurrents from a semiconductor solar cell chip near the micro-LED device during current injection. The main reasons for us to use a solar cell chip to collect red photons is because it can be in close proximity of the micro LED during the on-wafer test and this scheme can finish the basic photonic measurement in a very quick way without tedious dicing and packaging procedures. The GaAs-based solar cell chips were first tested for their external quantum efficiency by a 300-W Xenon lamp (Newport 66984) and a monochromator (Newport 74112) and then the 3000 μm $\times$ 3000 μm solar cell chip was attached to the tip of a probe on a 3-axis translational stage. When the photonic power measurement is needed, this custom-made probe can be moved to the device location and convert the received red photons into electrical currents picked up by a Keithley 2400 source meter. By the steps explained in the following section, we can calculate the equivalent quantum efficiency from this photocurrent measurement.

III. Measurements and Device Performance

A. Device Performance

After fabrication, the devices were tested through direct current injection. Fig. 2(a)–d presents the 2-, 5-, 10-, and 15-μm micro-LEDs under a current density of 100 A/cm^2. Although the larger devices were brighter, the illumination of the 2-μm device was visible under normal optical microscope illumination. The supplementary material contains an animation of the 2-μm device under various current injection levels (Visualization 1). Fig. 3(a) presents the devices' electrical characteristics and the current densities of devices of 2, 5, 10, and 15 μm are plotted in log scale for both forward and reversed bias regions. The 5-, 10-, and 15-μm devices had resistances of 58.7, 14.0, and 9.10 kΩ, respectively. The 2-μm device had, on the other hand, a wide range of distribution in electrical resistance. Its series resistance can be as high as several MΩ or as low as 9 kΩ in certain leaky devices. The working 2-μm devices we had have their resistances around 50 to 80 kΩ. From the J-V data of 5 to 15 μm devices, we saw a similar trend in forward bias compared to previous literatures, i.e., the smaller devices can hold a higher current density at the same voltage level [6], [25]. The only exception is the J-V characteristics of the 2 μm devices. Due to the difficulty to make a good contact on the mesa, 2-micron devices have a wide spread of current-voltage characteristics. As shown in Fig. 3(a), the IV can be very different from a

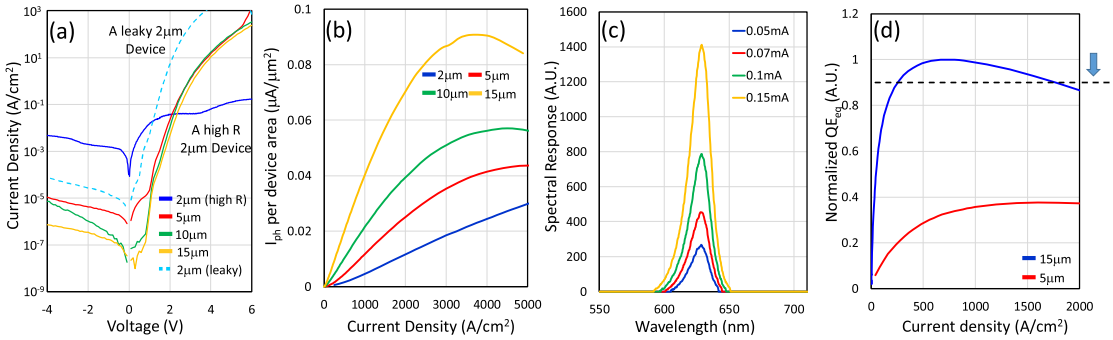

Fig. 3. (a) J-V characteristics of the red micro-LEDs. (b) Detected photocurrents of each micro-LED by injection current density. (c) Spectra of 15-μm device under various currents. (d) Normalized $QE_{\rm eq}$ for the 15-μm and 5-μm devices. The dashed line represents the approximate reduction in QE ($\sim$10%) at 100 A/cm^2 of the red LED devices in Royo *et al.* [12].

leaky diode to a highly resistive one. This variation illustrates the instability in our p-type contact patterning at this moment, and shall be the focus of the next improvement. At the reversed bias region, similar to what was reported, the leakage current densities tend to increase as the size of the device shrinks due to higher surface-to-volume ratio and the corresponding surface recombination [6], [8] and [25]. The reverse leakage at -4 volt of 2 μm devices can range from 7.71×10^{-5} A/cm^2 to 4.69×10^{-3} A/cm^2, while other devices (5 to 15 μm) have similar or lower leakage current compared to our previous results [6].

In addition to the IV characteristics, the light-emitting capabilities were evaluated through the photovoltaic current of a solar cell chip probe mentioned in Section II. The photocurrent of the solar cell chip can be converted to the emitted optical power of the micro-LED as follows [26]:

$$P_{opt} = \frac{I_{ph}}{\eta_{solar}} \times \frac{h\nu}{q}, \tag{1}$$

where $P_{\rm opt}$ is the incident optical power generated by the micro-LED device, $I_{\rm ph}$ is the measured photovoltaic current from the solar cell chip, $\eta_{\rm solar}$ is the external quantum efficiency of the solar cell, h is the Planck constant, ν is the frequency of the photons, and q is the elementary charge. The measured EQE ($\eta_{\rm solar}$) from the solar cell chip in the experiment in the red wavelength range was approximately 60%. Fig. 3(b) presents the photovoltaic current of each micro-LED by injection current density. From (1), the photovoltaic current is directly proportional to the received optical power from the micro LED. On the basis of GaN-related research, we expected that the small devices would have a high photonic power density [25], [27]. However, the results revealed the opposite; the areal illumination density, which is proportional to the photovoltaic current per unit area, of the small red micro-LEDs was low. To explain this opposite trend, we can examine the plot more closely. In Fig. 3(b), their slopes to the origin, which are similar to the wall-plug efficiencies of the devices, should be:

$$slope \propto \frac{P_{op}/A}{I/A}$$
$$= \frac{P_{op}}{I} = \frac{h\nu}{q} \times EQE = \frac{h\nu}{q} \times \eta_{LEE} \times IQE, \tag{2}$$

where $\eta_{\rm LEE}$ is the light extraction efficiency and IQE is the internal quantum efficiency. In previous publication, the IQEs of the devices are close and the improvement in the light extraction efficiency ($\eta_{\rm LEE}$) in the small devices can provide the enhanced wall-plug efficiency [25]. In our case, however, we face a different situation where the device quantum efficiency drops dramatically the mesa size shrinks. Meanwhile, the light extraction efficiency does not change much for vertical-sidewall devices smaller than 20 μm [28], [29]. If both factors are taken into account, as mesa shrinks, the overall product of $\eta_{\rm ext} \times$ IQE (and thus the slope in Fig. 3(b)) drops accordingly, and thus give us a reversed order in Fig. 3(b). In terms of rollover current density, for the large devices (10- and 15-μm devices), the photocurrent decreased as current density increased; these results are consistent with those of another study [27]. Fig. 3(c) presents the current-dependent spectra of the 15-μm device; the injection current was 0.05 to 0.15 mA. The shift in peak wavelength was similar to our previous observations, and a red shift at 0.34 nm was observed. The linewidth slightly widened from 16.17 to 18.44 nm.

B. Measuring the Devices' Quantum Efficiency

In addition to the regular properties of the micro LEDs, the efficiency of the device can also be calculated from the measured photovoltaic currents of the solar cell detector. The equivalent quantum efficiency ($\rm QE_{eq}$) of the micro-LED becomes:

$$QE_{eq} = \frac{Photons\ Emitted}{Injected\ Electron - hole\ pairs} = \frac{P_{opt}/h\nu}{I_{diode}/q}$$
$$= \frac{q}{h\nu} \frac{P_{opt}}{I_{diode}} = \frac{I_{ph}}{I_{diode} \times \eta_{solar}}, \tag{3}$$

where the $I_{\rm diode}$ is the electrical current injected into the micro-LED. Although the collection of the emitted red photons might not have been complete, the analysis could be continued by identifying the relative maximum of the current-dependent $QE_{\rm eq}$. Fig. 3d presents the current-dependent $QE_{\rm eq}$ of our micro-LEDs. Our devices displayed similar behavior in the low and medium current levels to that displayed by devices in another study [12]. In some cases, such as in the device reported by Royo *et al.* [12], a 10% decrease in efficiency was observed between its maximum value and that at 100 A/cm^2 (dashed). We did not observe this

decrease until current density exceeded 1500 A/cm^2 for the 15-μm device, and this range becomes even wider in smaller devices (5- and 2-μm devices). However, when the device began to roll over, the efficiency decreased rapidly at a rate beyond which the ordinary ABC model can handle. For this reason, we introduced the leakage current model, as described in the following section.

IV. Modified ABC Model With Consideration for Current Leakage

A. Revisiting the ABC Model and Current Leakage

The AlGaInP quantum well was investigated extensively in the 1980s and 1990s because of its role in semiconductor red lasers and LEDs. The leakage problem was discovered when an abnormal increase in the laser threshold current was reported [13]. Carrier leakage rises from the lack of sufficient potential confinement in the epitaxial structure of the device. Research has indicated that a low carrier confinement in the active region leads to carrier leakage and a subsequent decrease in efficiency [13], [15]. In the AlGaInP material system, the difficulty in achieving high p-type doping concentration [30], [31] and low electron potential barrier (the barrier height is around 0.185 eV reported in [13], and about 0.2 eV for a generic InGaAs/GaAs heterostructure [32], [33]) make the carrier leakage a greater concern. As the carrier obtain enough thermal energy and the potential barrier lowering occurs, it is easy for them to spread out of the active region and not to be radiatively recombined. The disparity between electron and hole mobility exacerbates the injection asymmetry of these two carriers and further reduce the radiative recombination efficiency [22]. Hence, the inherent small band offset and bias-dependent factors, like the injection asymmetry and the voltage drop in the p-type region, collaterally damage the photonic performance of AlGaInP LEDs at high current level, and we need to properly control this type of loss mechanism in the light emitting devices, such as LEDs and lasers, in order to make the device more efficient. The rate equations can be used to analyze the nonradiative and radiative processes in an LED [34]. In the ABC model, three terms are typically used for analysis: the Shockley–Read–Hall (SRH) recombination, the radiative recombination, and the Auger recombination. Although this is sufficient for general purposes, certain modifications are required to account for the material difference in AlGaInP devices. Leakage in the injection current is required in this material system, and to address this problem in micro-LEDs, a leakage current term can be added to the total current as follows [13], [15] and [22]:

$$J_{total} = qt\left(An + Bn^2 + Cn^3\right) + J_{leak}, \tag{4}$$

where J_{leak} is the leakage current component of the diode, q is the elementary charge, t is the thickness of the active region, A is the SRH coefficient, B is the bimolecular coefficient for radiative recombination, and C is the Auger recombination coefficient. In the literature, J_{leak} comprises two components: drift and diffusion [13], [31]. In general, when the current density is higher than 400 A/cm^2, the majority of the leakage current originates from the drift component of the injection current and is proportional to excess carrier concentration δn and total current J_{total}, expressed as follows [13], [22], [31] and [35]:

$$J_{leak} = \beta\delta n J_{total} = \ \beta n J_{total}, \tag{5}$$

where δn≈n is the excess carrier concentration, and β is related to the mobility of the carriers and the proportion of the carrier population that can overflow the active region [27].

After this is plugged into (4), the formula becomes

$$J_{total} = qt\left(An + Bn^2 + Cn^3\right) + \beta n J_{total}. \tag{6}$$

Unlike another study [27], in which a fourth-order term n^4 was used to approximate this leakage effect, the leakage component in our model was used to solve the equation by considering fitting parameter β and measurable quantity J_{total}. Upon further calculation, we discovered the following:

$$J_{total} = \frac{qt\left(An + Bn^2 + Cn^3\right)}{(1 - \beta n)} \tag{7}$$

EQE (or $\mathrm{QE_{eq}}$ in our case) can be calculated as follows:

$$QE_{eq} = \frac{\eta_{LEE}\left(1 - \beta n\right)Bn^2}{\left(An + Bn^2 + Cn^3\right)}, \tag{8}$$

where η_{LEE} is the light extraction efficiency and can be treated as a constant during calculation [36], [37]. By fitting the measured data and (8), we obtained A, B, C, and β. The absolute value of quantum efficiency of a small device is difficult to obtain, whereas the current density of the efficiency peak can be determined through this measurement method.

The Peak Value of Quantum Efficiency Can Be Found At the Carrier Concentration of

$$\mathrm{n}_{max} = \frac{-\beta A + \sqrt{(\beta A)^2 + A\left(C + \beta B\right)}}{\left(C + \beta B\right)} \tag{9}$$

which can be obtained by identifying the derivative zeros in (8). Compared with another study [27] in which $n_{\max}$ was expressed as $\sqrt{A/C}$, our expression in (9) is more complex because of the effect of the leakage current. Three scenarios for $(\beta A)^2$ and $A(C + \beta B)$ are possible in (8): $(\beta A)^2 >> A(C + \beta B)$, $(\beta A)^2 \approx A(C + \beta B)$, and $(\beta A)^2 << A(C + \beta B)$. After algebraic manipulation, we discovered the following:

$$n_{max} = \begin{cases} \frac{1}{2\beta}, \text{ if } (\beta A)^2 \gg A\left(C + \beta B\right); \\ \left(\sqrt{2} - 1\right)\sqrt{\frac{A}{C+\beta B}}, \text{ if } (\beta A)^2 \approx A\left(C + \beta B\right); \\ \sqrt{\frac{A}{C+\beta B}}, \text{ if } (\beta A)^2 \ll A\left(C + \beta B\right); \end{cases} \tag{10}$$

Among these three conditions, $n_{\max}$ becomes proportional to $\sqrt{A/(C + \beta B)}$ in two conditions; this is similar to the no-leak case but with a modified leakage term. The value of the maximum carrier concentration approximates $1/(2\beta)$ in the case of $(\beta A)^2 >> A(C + \beta B)$.

After the current leakage–based model was constructed, we first examined the difference in the effect of quantum efficiency due to the change in the parameters in the formula. Fig. 4(a) presents the numerical effect of β, which varies from 2×10^{-24} to 6×10^{-25} m^3. As expected, the higher β is, the lower

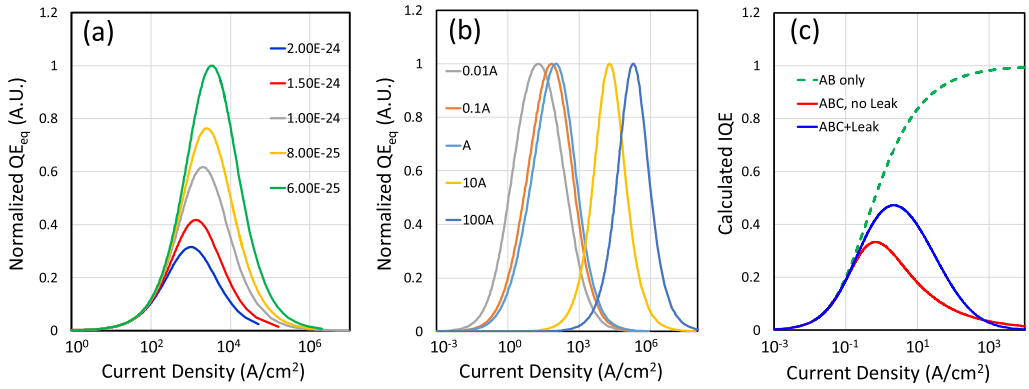

Fig. 4. QE$_{eq}$ (a) Under various β values and (b) Under various SRH coefficients (where $A = 5.99 \times 10^8$ 1/sec). (c) Various ABC models: AB only, ABC without current leakage component, and ABC with current leakage component. The slopes of the ABC models with and without the current leakage component differ under high current densities.

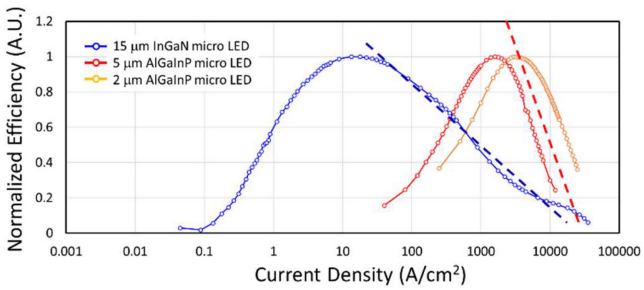

Fig. 5. The comparison between the equivalent EQEs of InGaN (blue) and AlGaInP (red) micro LEDs. The dashed lines provide guides for the eye and different slopes of reduction in efficiency can be observed.

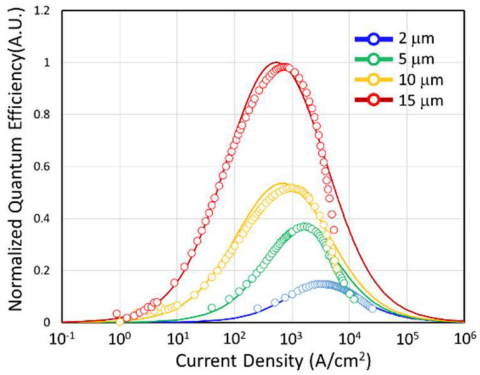

Fig. 6. Normalized QE$_{eq}$ for each micro-LED. The dots represent the measured results, and the lines represent the results of calculation with (8). The efficiency decreases under high current densities for all micro-LEDs.

QE$_{eq}$ is. The change in the SRH coefficient, A, resulted in a dramatic shift in J_{max}, which represents the current density at the maximal QE$_{eq}$ (Fig. 4(b)). This result can be referenced in subsequent studies of the SRH recombination of our devices. Because deviation may occur in the magnitude of the detected photocurrent and consequently in the absolute value of QE$_{eq}$, the J_{max} is more accurate and can be used to evaluate the SRH coefficient.

Fig. 4(c) presents the various mechanisms and the quantum efficiency by current density. In this figure, the ordinary ABC model (with and without Auger recombination) and our leakage–based model are put together under the same set of parameters for comparison. For this calculation, we set A to 10^7 1/sec, B to 10^{-11} cm^3/sec, C to 10^{-30} cm^6/sec, and β to 10^{-25} m^3. The dashed line represents no Auger recombination (only A and B coefficients) and the highest quantum efficiency [14]. The normal ABC model (red curve) exhibited a slow decrease in efficiency at high current densities. Our modified model with the current leakage component exhibited similar quantum efficiencies at low and medium current densities, but quantum efficiency decreased rapidly at high current densities.

B. Comparison With Experimental Results

In this section, we will compare the experimental results with our new model. First, the necessity to include leakage current into our model can be seen in Fig. 5, where the experimental results between AlGaInP and InGaN (blue) micro LEDs are compared. From the data measured by the same method and the same solar cell chip, we are able to observe the different decline rates of the two types of devices. In the blue micro LEDs, where the original ABC model applies and the Auger recombination (CN^3 term) dominates, the normalized quantum efficiency can drop proportionally to N^{-1} at high current density. Meanwhile, the reduction in efficiency of AlGaInP LEDs is greatly accelerated by the current leakage and can only be described properly by an extra term of (1-βN) in our modified model, as stated in (8).

Then the model data were matched with our experimental results for the smaller micro-LEDs. QE$_{eq}$ in Fig. 6 was measured using the aforementioned solar cell chip, and the optical power was estimated using (1) and (3). The results of QE$_{eq}$ normalization indicated that the efficiency of the 2-μm device is approximately 6.7 times lower than that of the 15-μm device. The QE$_{eq}$ of all devices decreased considerably as current density increased; this phenomenon cannot be suitably matched using the normal ABC model. Table I presents the corresponding parameters of the SRH coefficients and β values in Fig. 6.

From Table 1, larger numerical values of β can be observed for smaller devices. Many papers have shown the serious carrier leakage existed in this material [13], [38] and [39], and the

TABLE I
CORRESPONDING SRH COEFFICIENTS AND β VALUES IN FIG. 6 FOR EACH DEVICE

Fitted results	*2 μm*	*5 μm*	*10 μm*	*15 μm*
A (1/sec)	4.25×10^{9}	1.85×10^{9}	2.16×10^{8}	1.66×10^{8}
β	4×10^{-24}	4×10^{-24}	1×10^{-24}	1×10^{-24}

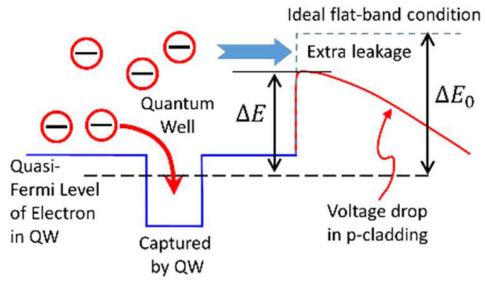

Fig. 7. Schematic diagram of electron leakage under the flat-band condition (dashed line) and the barrier lowering case (red).

carrier leakage follows a similar relationship on current. As the bias increases, the leakage tends to increase. As pointed out by previous publication [13], the leakage current for electrons in a heterojunction device can be formulated as:

$$J_L = qD_nN_0\left(J_{diff} + J_{drift}\right), \tag{11}$$

where D_n is the minority electron diffusion coefficient, J_{diff} and J_{drift} are the diffusion and drift components in the leakage, and N_0 can be further explained as:

$$N_0 = 2\left(\frac{m_n^* kT}{2\pi\hbar^2}\right)^{3/2} e^{-\frac{\Delta E}{kT}}, \tag{12}$$

and ΔE is the effective potential barrier at the heterojunction as shown in Fig. 7. When the device is biased under forward direction, the voltage drop in the p-type region becomes important. If the voltage drop in the p-type region is small, as assumed by most of the textbooks, the leakage current is defined by the full band offset (ΔE_0). However, if certain voltage drop happens in the p-type region, the lowering of the band offset can occur as we increase the bias to the device. This lowering in barrier can lead to the increase of N_0 through (12) and thus causing more carrier leakage than the flat-band condition which does not have any voltage drop in p-type region. In our micro LED case, when the device gets smaller, due to the rise of series resistance shown in J-V characteristics (such as Fig. 3(a)), it is possible that the voltage drop in the p-type region for the smaller devices can increase and thus the acquired values of β is larger for smaller devices in Table 1.

With the extraction of critical parameters in Table 1, we can further use them to explore the SRH recombination in these small devices. From the observation in Fig. 6, J_{max} shifted toward high current densities in the smaller devices, and a larger SRH coefficient (A) is obtained. In most cases, the current density at the peak efficiency can reflect the magnitude of SRH recombination coefficient A; and this can be evaluated through our measurement method. The extracted values of the SRH coefficient for each micro-LED can be plotted against the inverse of side length (Fig. 8). Similar to the results of another study [24], the average value of the measured SRH coefficient was lower for the larger device. The SRH coefficients can be expressed as follows [12], [24]:

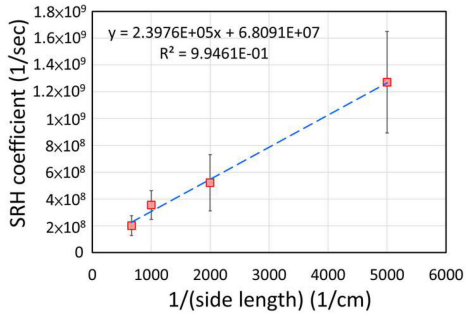

Fig. 8. SRH coefficient vs. inverse of side length in a linear relationship, as predicted by (13). Error bars represent standard deviation.

$$A = A_0 + \frac{4v_s}{\sqrt{S_{mesa}}} = A_0 + \frac{4v_s}{L_{mesa}}, \tag{13}$$

where A_0 is the bulk SRH value, v_s is the surface recombination velocity, S_{mesa} is the area of the device mesa, and L_{mesa} is the side length of the mesa. The fitting results indicated that an A_0 of 6.81×10^7 1/sec can be obtained. The surface recombination velocity was 5.99×10^4 cm/sec, which is within the ranges reported for GaInP and AlInP compound semiconductors [34], [40] and [41]. The bulk SRH value can vary by growth technology and wafer runs between 2×10^7 and 10^8 1/sec [21], [42], and our A_0 value was within this range.

V. CONCLUSION

We fabricated and investigated the efficiency of AlGaInP red micro-LEDs ranging from 2 to 15 μm in size, which will be critical in augmented and virtual reality and high-resolution microdisplays. The current-dependent efficiency decreased sharply at high current densities; this might have resulted from the low carrier confinement potential in the material system. The addition of a leakage component to the ABC model helped the calculated values approximate the experimental data. The extracted SRH parameters and surface recombination velocity also coincided with reported values. This modified model will be useful for the next generation of AlGaInP-based micro-LEDs.

ACKNOWLEDGMENT

The authors would like to thank Prof. Cheng-Huang Kuo and Prof. Kuo-Ping Chen of National Yang Ming Chiao Tung University, Prof. Jinn-Kong Sheu and Prof. Wei-Chih Lai of National Cheng Kung University for their technical supports.

REFERENCES

[1] J. Y. Lin and H. X. Jiang, "Development of microLED," *Appl. Phys. Lett.*, vol. 116, no. 10, pp. 100502, 2020, doi: 10.1063/1.5145201.
[2] P. J. Parbrook, B. Corbett, J. Han, T.-Y. Seong, and H. Amano, "Micro-light emitting diode: From chips to applications," *Laser Photon. Rev.*, vol. 15, no. 5, 2021, Art. no. 2000133, doi: 10.1002/lpor.202000133.

[3] K. Kishino, N. Sakakibara, K. Narita, and T. Oto, "Two-dimensional multicolor (RGBY) integrated nanocolumn micro-LEDs as a fundamental technology of micro-LED display," *Appl. Phys. Exp.*, vol. 13, no. 1, Dec. 2019, Art. no. 014003, doi: 10.7567/1882-0786/ab5ad3.

[4] J. J. Wierer Jr. and N. Tansu, "III-nitride micro-LEDs for efficient emissive displays," *Laser Photon. Rev.*, vol. 13, no. 9, 2019, Art. no. 1900141, doi: 10.1002/lpor.201900141.

[5] Z. Zhuang, D. Iida, M. Velazquez-Rizo, and K. Ohkawa, "630-nm red InGaN micro-light-emitting diodes ($<$20 μm $\times$ 20 μm) exceeding 1 mW/mm^2 for full-color micro-displays," *Photon. Res.*, vol. 9, no. 9, pp. 1796–1802, Sep. 2021, doi: 10.1364/PRJ.428168.

[6] H.-H. Huang *et al.*, "Investigation on reliability of red micro-light emitting diodes with atomic layer deposition passivation layers," *Opt. Exp.*, vol. 28, no. 25, pp. 38184–38195, Dec. 2020, doi: 10.1364/OE.411591.

[7] M. S. Wong *et al.*, "High efficiency of III-nitride micro-light-emitting diodes by sidewall passivation using atomic layer deposition," *Opt. Exp.*, vol. 26, no. 16, pp. 21324–21331, Aug. 2018, doi: 10.1364/OE.26.021324.

[8] M. S. Wong *et al.*, "Improved performance of AlGaInP red micro-light-emitting diodes with sidewall treatments," *Opt. Exp.*, vol. 28, no. 4, pp. 5787–5793, Feb. 2020, doi: 10.1364/OE.384127.

[9] Y. Zhao *et al.*, "2000 PPI silicon-based AlGaInP red micro-LED arrays fabricated via wafer bonding and epilayer lift-off," *Opt. Exp.*, vol. 29, no. 13, pp. 20217–20228, Jun. 2021, doi: 10.1364/OE.428482.

[10] J. M. Smith *et al.*, "Comparison of size-dependent characteristics of blue and green InGaN microLEDs down to 1 μm in diameter," *Appl. Phys. Lett.*, vol. 116, no. 7, 2020, Art. no. 071102, doi: 10.1063/1.5144819.

[11] J. Park *et al.*, "Electrically driven mid-submicrometre pixelation of InGaN micro-light-emitting diode displays for augmented-reality glasses," *Nature Photon.*, vol. 15, no. 6, pp. 449–455, Jun. 2021, doi: 10.1038/s41566-021-00783-1.

[12] P. Royo, R. P. Stanley, M. Ilegems, K. Streubel, and K. H. Gulden, "Experimental determination of the internal quantum efficiency of AlGaInP microcavity light-emitting diodes," *J. Appl. Phys.*, vol. 91, no. 5, pp. 2563–2568, 2002, doi: 10.1063/1.1433938.

[13] D. P. Bour, D. W. Treat, R. L. Thornton, R. S. Geels, and D. F. Welch, "Drift leakage current in AlGaInP quantum-well lasers," *IJQE*, vol. 29, no. 5, pp. 1337–1343, 1993, doi: 10.1109/3.236147.

[14] A. Yadav *et al.*, "Temperature effects on optical properties and efficiency of red AlGaInP-based light emitting diodes under high current pulse pumping," *J. Appl. Phys.*, vol. 124, no. 1, 2018, Art. no. 013103, doi: 10.1063/1.5020266.

[15] P. Altieri *et al.*, "Internal quantum efficiency of high-brightness AlGaInP light-emitting devices," *J. Appl. Phys.*, vol. 98, no. 8, 2005, Art. no. 086101, doi: 10.1063/1.2085308.

[16] J.-T. Oh *et al.*, "Light output performance of red AlGaInP-based light emitting diodes with different chip geometries and structures," *Opt. Exp.*, vol. 26, no. 9, pp. 11194–11200, Apr. 2018, doi: 10.1364/OE.26.011194.

[17] A. Gin, Y. Wei, J. Bae, A. Hood, J. Nah, and M. Razeghi, "Passivation of type II InAs/GaSb superlattice photodiodes," *Thin Solid Films*, vol. 447-448, pp. 489–492, Jan. 2004, doi: 10.1016/j.tsf.2003.09.002.

[18] E. A. Plis, M. N. Kutty, and S. Krishna, "Passivation techniques for InAs/GaSb strained layer superlattice detectors," *Laser Photon. Rev.*, vol. 7, no. 1, pp. 45–59, 2013, doi: 10.1002/lpor.201100029.

[19] M. Wong, J. Speck, S. Nakamura, and S. DenBaars, *High Efficiency III-Nitride AlGaInP Micro-Light-Emitting Diodes Using Atomic Layer Deposition (SPIE OPTO)*, SPIE, 2021.

[20] M. Herrera *et al.*, "Atomic scale analysis of the effect of the SiO_2 passivation treatment on InAs/GaSb superlattice mesa sidewall," *Appl. Phys. Lett.*, vol. 93, no. 9, 2008, Art. no. 093106, doi: 10.1063/1.2977589.

[21] E. E. Perl, D. Kuciauskas, J. Simon, D. J. Friedman, and M. A. Steiner, "Identification of the limiting factors for high-temperature GaAs, GaInP, and AlGaInP solar cells from device and carrier lifetime analysis," *J. Appl. Phys.*, vol. 122, no. 23, 2017, Art. no. 233102, doi: 10.1063/1.5003631.

[22] J.-I. Shim *et al.*, "Efficiency droop in AlGaInP and GaInN light-emitting diodes," *Appl. Phys. Lett.*, vol. 100, no. 11, 2012, Art. no. 111106, doi: 10.1063/1.3694044.

[23] P. M. Smowton and P. Blood, "The differential efficiency of quantum-well lasers," *IEEE J. Sel. Top. Quant.*, vol. 3, no. 2, pp. 491–498, Apr. 1997, doi: 10.1109/2944.605699.

[24] F. Olivier, A. Daami, C. Licitra, and F. Templier, "Shockley-Read-Hall and auger non-radiative recombination in GaN based LEDs: A size effect study," *Appl. Phys. Lett.*, vol. 111, no. 2, 2017, Art. no. 022104, doi: 10.1063/1.4993741.

[25] Z. Gong *et al.*, "Size-dependent light output, spectral shift, and self-heating of 400 nm InGaN light-emitting diodes," *J. Appl. Phys.*, vol. 107, no. 1, 2010, Art. no. 013103, doi: 10.1063/1.3276156.

[26] S. M. Sze, *Physics of Semiconductor Devices*, 2nd ed. New York, NY, USA: Wiley, 1981.

[27] G.-B. Lin, D. Meyaard, J. Cho, E. F. Schubert, H. Shim, and C. Sone, "Analytic model for the efficiency droop in semiconductors with asymmetric carrier-transport properties based on drift-induced reduction of injection efficiency," *Appl. Phys. Lett.*, vol. 100, no. 16, 2012, Art. no. 161106, doi: 10.1063/1.4704366.

[28] K. A. Bulashevich, S. S. Konoplev, and S. Y. Karpov, "Effect of die shape and size on performance of III-nitride micro-LEDs: A modeling study," *Photonics*, vol. 5, no. 4, 2018, Art. no. 41. [Online]. Available: https://www.mdpi.com/2304-6732/5/4/41

[29] R. T. Ley *et al.*, "Revealing the importance of light extraction efficiency in InGaN/GaN microLEDs via chemical treatment and dielectric passivation," *Appl. Phys. Lett.*, vol. 116, no. 25, 2020, Art. no. 251104, doi: 10.1063/5.0011651.

[30] T. Yokotsuka, A. Takamori, and M. Nakajima, "Growth of heavily be-doped AlInP by gas source molecular beam epitaxy," *Appl. Phys. Lett.*, vol. 58, no. 14, pp. 1521–1523, 1991, doi: 10.1063/1.105165.

[31] F. A. Kish and R. M. Fletcher, "AlGaInP light-emitting diodes," in *Semiconductors and Semimetals*, vol. 48, G. B. Stringfellow and M. G. Craford, Eds., Amsterdam, The Netherlands: Elsevier, 1997.

[32] G. Karunasiri, "Thermionic emission and tunneling in InGaAs/GaAs quantum well infrared detectors," *J. Appl. Phys.*, vol. 79, no. 10, pp. 8121–8123, 1996, doi: 10.1063/1.362372.

[33] I. Vurgaftman, J. R. Meyer, and L. R. Ram-Mohan, "Band parameters for III–V compound semiconductors and their alloys," *J. Appl. Phys.*, vol. 89, no. 11, pp. 5815–5875, 2001, doi: 10.1063/1.1368156.

[34] L. A. Coldren and S. W. Corzine, *Diode Lasers and Photonic Integrated Circuits.* ser. Wiley Series in Microwave and Optical Engineering. New York, NY, USA: Wiley, 1995.

[35] J. Cho, E. F. Schubert, and J. K. Kim, "Efficiency droop in light-emitting diodes: Challenges and countermeasures," *Laser Photon. Rev.*, vol. 7, no. 3, pp. 408–421, 2013, doi: 10.1002/lpor.201200025.

[36] C. Tian, W. Wang, J. Liang, Z. Liang, Y. Qin, and J. Lv, "Theoretical and experimental analysis of AlGaInP micro-LED array with square-circle anode," *AIP Adv.*, vol. 5, no. 4, 2015, Art. no. 041309, doi: 10.1063/1.4904217.

[37] A. Daami and F. Olivier, "InGaN/GaN µLED SPICE modelling with size dependent ABC model integration," in *Proc. InGaN/GaN µLED SPICE Modelling With Size-Dependent ABC Model Integration (SPIE OPTO)*, SPIE, 2019.

[38] K. Streubel, N. Linder, R. Wirth, and A. Jaeger, "High brightness AlGaInP light-emitting diodes," *IEEE J. Sel. Top. Quant.*, vol. 8, no. 2, pp. 321–332, Aug. 2002, doi: 10.1109/2944.999187.

[39] P. Kivisaari *et al.*, "Optimization of current injection in AlGaInP core−shell nanowire light-emitting diodes," *Nano Lett.*, vol. 17, no. 6, pp. 3599–3606, Jun. 2017, doi: 10.1021/acs.nanolett.7b00759.

[40] K. A. Bulashevich and S. Y. Karpov, "Impact of surface recombination on efficiency of III-nitride light-emitting diodes," *Physica status solidi (RRL) – Rapid Res. Lett.*, vol. 10, no. 6, pp. 480–484, 2016, doi: 10.1002/pssr.201600059.

[41] S. J. Pearton, F. Ren, W. S. Hobson, C. R. Abernathy, and U. K. Chakrabarti, "Effects of wet and dry etching and sulphide passivation on surface recombination velocities of InGaP p-n junctions," in *Proc. 1994 IEEE 6th Int. Conf. Indium Phosphide Related Mater.*, Mar. 1994, pp. 186–189, doi: 10.1109/ICIPRM.1994.328193.

[42] M. Niemeyer *et al.*, "Measurement of the non-radiative minority recombination lifetime and the effective radiative recombination coefficient in GaAs," *AIP Adv.*, vol. 9, no. 4, 2019, Art. no. 045034, doi: 10.1063/1.5051709.